Stability analysis and break–up length calculations for steady planar liquid jets.

By M. R. TURNER[1]†, J. J. HEALEY[2], S. S. SAZHIN[1] AND R. PIAZZESI[1]

[1] Sir Harry Ricardo Laboratories, School of Computing, Engineering and Mathematics, University of Brighton, Lewes Road, Brighton BN2 4GJ UK
[2] Department of Mathematics, Keele University, Keele, Staffs ST5 5BG UK

(Received 9 September 2010)

This study uses spatio–temporal stability analysis to investigate the convective and absolute instability properties of a steady unconfined planar liquid jet. The approach uses a piecewise linear velocity profile with a finite thickness shear layer at the edge of the jet. This study investigates how properties such as the thickness of the shear layer and the value of the fluid velocity at the interface within the shear layer affects the stability properties of the jet. It is found that the presence of a finite thickness shear layer can lead to an absolute instability for a range of density ratios, not seen when a simpler plug flow velocity profile is considered. It is also found that the inclusion of surface tension has a stabilizing effect on the convective instability but a destabilizing effect on the absolute instability.

The stability results are used to obtain estimates for the break–up length of a planar liquid jet as the jet velocity varies. It is found that reducing the shear layer thickness within the jet causes the break–up length to decrease, while increasing the fluid velocity at the fluid interface within the shear layer causes the break–up length to increase. Combining these two effects into a profile, which evolves realistically with velocity, gives results in which the break–up length increases for small velocities and decreases for larger velocities. This behaviour agrees qualitatively with existing experiments on the break–up length of axisymmetric jets.

1. Introduction

The injection of Diesel fuel into an engine cylinder is an important process in the overall running and efficiency of a Diesel engine (Hiroyasu *et al.* 1982; Stone 1992; Heywood 1998; Crua 2002). The liquid fuel is injected through an injector (which can have multiple holes) and the resulting jet breaks up into small droplets. These droplets heat up, evaporate and the mixture of fuel vapour and air burns up in the autoignition and combustion processes. During the injection process a useful quantity to predict, or measure, is the break–up length of the jet. This is the length over which the jet remains intact before it begins to break up into ligaments and droplets. Modelling this injection process is an important integral part of the CFD Diesel engine models (Sazhin *et al.* 2003, 2008). During the injection process these jets undergo acceleration, but, like most current injection models, we neglect this process and in this paper we give a more complete analysis of the steady jet problem by studying parameter ranges that cover those seen in Diesel injection models, as well as extending the research to look at parameters that cover a wider range of jets

† Corresponding author: M.R.Turner@brighton.ac.uk

which will be of interest to problems outside of Diesel injection problems. Furthermore, when the jet acceleration is relatively weak, the jet may be treated using a quasi–steady approximation which can give some qualitative insight into how acceleration may affect break–up. Thus this analysis is expected to help with future studies of the unsteady jet problem. While the jets in Diesel engines are close to axisymmetric jets, in this paper we consider only planar jets as these allow us to greatly simplify the analysis and lead to analytical results. The stability and break–up properties of both axisymmetric and planar jets has been studied both experimentally and theoretically in the past, and for a good overview of these studies the reader is directed to the introduction of Söderberg & Alfredsson (1998).

A planar jet consists of two parallel shear layers where the vorticity at each layer is equal and opposite. The stability properties of such jets are found by performing a linear stability analysis about a basic velocity profile $U(y)$ where y is a coordinate normal to the jet axis. By looking for a traveling wave solution of the linearized Navier–Stokes equations of the form $\hat{v}(x,y,t) = v(y)\exp[i(\alpha x - \omega t)]$, in the absence of viscosity, we arrive at the Rayleigh equation

$$(\alpha U - \omega)\left(\frac{d^2 v}{dy^2} - \alpha^2 v\right) - \alpha \frac{d^2 U}{dy^2} v = 0, \tag{1.1}$$

where $v(y)$ is the velocity component normal to the jet axis (in y–direction), t is time, α is the streamwise wavenumber and ω is the angular frequency; see Drazin & Reid (1981). Here we neglect the effect of viscosity as typical Reynolds numbers for Diesel jets are $O(10^4)$ or larger, which is larger than, 10^3, a value above which viscosity can be neglected in channel flows (Rees & Juniper 2010). Using a piecewise linear profile for $U(y)$ allows an analytic form of the dispersion relation $D(\alpha,\omega) = 0$ to be derived, on which a temporal stability analysis can be performed. The dispersion relation can be solved for complex ω, for a given real α. For the case of planar and axisymmetric jets, the range of real wavenumbers which exhibit growth is governed by the width of the shear layer and the magnitude of the surface tension (Lord Rayleigh 1894; Batchelor & Gill 1962; Funada *et al.* 2004; Marmottant & Villermaux 2004). However, a temporal stability analysis does not show certain aspects of the jet stability, such as whether or not it is absolutely or convectively unstable, which has important implications for where it breaks up. The answer to this question requires a different mathematical approach.

This approach uses spatio–temporal stability analysis (Heurre & Monkewitz 1990) in which both α and ω are allowed to become complex and growth rates are obtained in various frames of reference moving in the axial direction along the jet. The growth rate is calculated using the method of steepest descent (Hinch 1991) by searching for special saddle points in the complex $\alpha-$plane through which the inverse Fourier transform contour can be deformed (see §2.1). The saddle point on the contour with the largest growth rate gives the disturbance growth rate in the limit $t \to \infty$. For a liquid jet there is one saddle point in the $\alpha-$plane whose position is determined by the thickness of the shear layers and the value of the surface tension (known as the 's_1' saddle in Juniper (2007) and 'shear layer mode' in Lesshafft & Huerre (2007)), and this saddle is located close to the real $\alpha-$axis. Also in the $\alpha-$plane is a set of saddle points close to the imaginary $\alpha-$axis which are due to the interaction between the two shear layers (known as 's_2' saddles in Juniper (2007) and 'jet column modes' in Lesshafft & Huerre (2007)). In the present study we examine how the growth rate at these saddles and their positions are affected when the interface between the two fluids is placed within the shear layer. We find that this leads to important qualitative differences compared to previous studies where the density interface was assumed to lie on only one side of the shear layer (Marmottant

& Villermaux 2004; Juniper 2007). Our assumption to neglect viscosity in this study is valid because Yu & Monkewitz (1990) showed that the transition to absolute instability is caused by the interaction between the two shear layers and is not a viscous effect. Lin *et al.* (1990) and Li & Tankin (1991) investigated the effect of viscosity on planar liquid jets and found that the solution contained two convectively unstable modes, identical to those of Hagerty & Shea (1955), whose growth rates are affected by the presence of the viscosity, and an unstable mode with zero frequency. Typically viscosity has a damping effect on the instabilities, but in particular parameter regimes viscosity enhances one of the convective modes (Li & Tankin 1991).

The parameters we wish to investigate in this study are $q = \rho_2/\rho_1$, the density ratio of the outer fluid to that of the liquid jet, $W = We^{-1}$, the inverse Weber number (defined below), δ_1 and δ_2 the thicknesses of the shear layers on either side of the fluid interface and the ratio of the fluid velocity at the interface to the maximum jet velocity, β. It is known that the density ratio has a large effect on the behaviour of absolute instabilities, in particular that low density jets ($q > 1$) are almost always absolutely unstable (Sreenivasan *et al.* 1989; Yu & Monkewitz 1990; Juniper 2006). In this work we are concerned with jets which have $q < 1$, but we find that absolute instabilities can occur at these density ratios for particular velocity profiles. Values of $q < 1/10$ can typically be found in Diesel jet injection experiments as the pressure of the gas inside the cylinder is varied, while values of $q > 1/10$ provide a wider range of interest to the reader. Rees & Juniper (2009) showed that the effect of small and moderate surface tension values is to increase the magnitude of any absolute instability that arises due to the varicose modes of low density jets, while larger surface tension values are ultimately a stabilizing feature of the flow. This is one of the main differences between planar jets and axisymmetric jets, where surface tension has a more destabilizing effect. The effect of the shear layers in both fluids, and the magnitude of the fluid velocity at the fluid interface, on the absolute instability properties of jets with $q < 1$ has not been explored to date and will form part of this investigation. The case of low density jets ($q > 1$) with a fluid interface in the shear layer has been examined using smooth velocity and density profiles (Raynal *et al.* 1996; Srinivasan *et al.* 2010). These studies show that low density jets experience a transition from absolute to convective instability if the shear layer thickness is sufficiently large compared to the jet diameter.

The stability results are then used to estimate break–up lengths of steady jets, which are compared with experiments such as those of Hiroyasu *et al.* (1982). The experiments show that break–up lengths increase with injection velocity for small injection velocities and then reduce for larger velocities before eventually leveling off (see figure 13 of Hiroyasu *et al.* (1982) which is reproduced as figure 1 here). In the comprehensive review paper by Eggers & Villermaux (2008) the reducing break–up length for larger velocities is explained by the thinning shear velocity at the edge of the jet, but no explanation is given for the rise in break–up length for small velocities. In this paper we show that the increasing break–up length for small velocities could be due to the value of the fluid velocity at the fluid interface within the shear layer increasing with velocity. The experiments of Hiroyasu *et al.* (1982) are not performed using Diesel jets, but this experiment has non–dimensional parameters which coincide with those we expect in Diesel injection systems.

The present paper is laid out as follows. In §2 we formulate the problem and derive the analytic dispersion relation which determines the stability characteristics of the jet. Then follows a brief discussion of the spatio–temporal stability method used to analyze the jet stability, including in §2.2 a discussion of the s_1 and s_2 saddle points in the complex $\alpha-$plane and how they move around as the problem parameters vary. In §3 we calculate

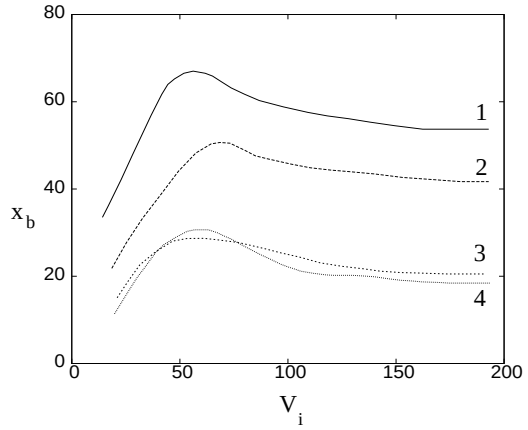

FIGURE 1. Plot of the break–up length x_b (mm) as a function of the injection velocity, v_i (ms^{-1}), for an experiment where water is injected into pressurized Nitrogen (Hiroyasu *et al.* 1982). The results are for four different Nitrogen pressures, which correspond to $q \approx 1/1000$, $1/100$, $1/30$ and $1/20$. These are numbered 1–4 respectively. The radius of the nozzle used in this experiment was 0.15mm.

the growth rates for particular parameter regimes and investigate the appearance or otherwise of absolute instabilities. In §4 we use the convective instability analysis to examine the break–up length of a steady liquid jet, and compare the results to those in figure 1. Our concluding remarks and discussion can be found in §5

2. Formulation of the mathematical model

We consider a two–dimensional steady planar jet orientated along the x^*-axis in the (x^*, y^*) plane with dimensional reference velocity U_0^* at $y^* = 0$, emerging from a nozzle of thickness $2L^*$ at $x^* = 0$. Using this reference length and velocity we can define dimensionless variables such as its velocity U =velocity of the jet/U_0^* and its thickness $2L$ (where L =thickness of the jet/$2L^*$). The jet fluid has density ρ_1 and lies between an outer fluid of density ρ_2. For the stability analysis in §3 we consider a jet profile with $\max(U) \equiv V = 1$, however when we consider break–up lengths for these jets in §4, we will allow V to vary. Thus we leave V explicitly in the equations in this section for completeness.

We assume that the jet does not spread significantly as we move along the $x-$axis in the region we wish to consider, and we neglect any streamwise variation of the jet in this article. Therefore we can consider the basic velocity profile $\mathbf{u} = U(y)\mathbf{i}$ as a function of the normal coordinate y only, where $\mathbf{i}$ is the unit vector in the streamwise direction. This assumption is valid close to the nozzle, where the jet spreads slowly in space. Typically this velocity profile will be smooth with shear layers in each fluid at the edge of the jet, such as in the CFD simulations in figure 2. The velocity profiles in figure 2(a) are calculated for an axisymmetric Diesel jet injecting in static air, normalised by their axial velocity along the centre of the jet, and non–dimensionalised by the radius of the nozzle ($L^* = 0.0675$ mm). These profiles are generated using the CFD package ANSYS® FLUENT®, where the boundary condition for the mass flow rate of fluid in the nozzle is given by measurements taken from an in house experiment (see figure 2(b)) (Karimi 2007). The plotted profiles are taken at $t^* = 3 \times 10^{-4}$ s where the jet has reached a steady state.

The velocity profiles in figure 2 are calculated using the Eulerian multiphase model. In

this model a momentum equation for each fluid phase is solved for, giving the respective velocity field. Since there exist large velocity differences between the two phases, this approach allows us to overcome the limitations of the shared velocity and temperature formulation of the Volume of fluid model (VOF), which can affect the fluid velocities computed across the interface. We consider the two fluids to be immiscible and the Geo–Reconstruction sharpening scheme (Youngs 1982; Ferziger & Peric 2004) is used to construct the free surface. The computational domain is a closed cylinder 80 mm in length and 25 mm in the radial direction which was chosen to approximate the cylinder of an engine in the experimental facilities at the University of Brighton. The nozzle is approximated by a cylindrical channel of $1.08\ \text{mm} \times 0.135\ \text{mm}$ (axial $\times$ radial directions) and is located at the centre of the main cylinder edge. The computational domain is covered by a structured mesh of approximately 82000 nodes which is refined inside the nozzle and in a $0.5\ \text{mm} \times 0.3\ \text{mm}$ region immediately outside the nozzle. A coarser and unstructured mesh is used outside this region and a time step of $\Delta t^* = 5 \times 10^{-8}$ s is used. A standard $\kappa - \epsilon$ turbulent model for both fluids is used. Initially the air in the chamber is considered at rest with a temperature of 355 K and a pressure of 2 MPa. The fuel is injected into the cylinder through the nozzle at the constant temperature of 355 K, assuming an adiabatic condition on the walls and applying a mass flow rate boundary condition, given by figure 2(b), at the nozzle inlet surface. This produces a non–uniform velocity profile as the fuel enters the main cylinder. A check of the dependency of the results on the numerical grid was also carried out and the results were found to agree within a few percent, hence the simulations are consistent.

The mass flow rate in figure 2(b) has been modified so that it levels off once the initial acceleration of the jet has been completed at around $t^* = 2.5 \times 10^{-4}$ s. Beyond this time the jet reaches a steady state, although from $t^* = 2.5 \times 10^{-4}$ s onwards, the change in the profiles is very small. The other profiles are generated by considering fractional multiples of this mass flow rate to generate the lower velocity jets. These profiles are generated assuming that the jet is axisymmetric, but we expect qualitatively similar results for a planar jet, so we use these results to motivate the velocity profiles used in this study. In fact the experimental results of Söderberg & Alfredsson (1998) show planar jet velocity profiles which have a similar appearance to those shown here, however they cannot determine the structure of the velocity profile in the outer fluid as we can in our CFD simulations. The profiles in figure 2(a) are taken at 0.1 mm from the nozzle exit and the nozzle is assumed to be full of fluid for all times to best model the flow in a Diesel injector where the nozzle fills with fluid as the injector needle is lifted. In this study we approximate the CFD profiles in figure 2 by a piecewise linear velocity profile, which is shown in figure 3. Although this profile is a simplification of the true profile, it captures important qualitative aspects of the jet, and greatly simplifies the problem when it comes to studying properties such as absolute instabilities. This piecewise linear profile exhibits the same qualitative behaviour as a realistic smooth profile, as the exact shape of the shear layer only has a small effect on the stability characteristics of the flow (Esch 1957), and Healey (2009) found a co–flow absolute instability for certain confined piecewise linear shear layers and the same qualitative behaviour, with modest quantitative variation, in smooth profiles. The piecewise linear profile also allows for an analytical expression for the dispersion relation, as well as implicitly capturing typical features of a viscous jet profile, although we do not explicitly consider the effects of viscosity in this model. Other studies have considered the stability of planar jets using velocity profiles which are more realistic, i.e. have shear layers either side of the fluid interface, than the simple plug flow approximation (Hashimoto & Suzuki 1991; Söderberg & Alfredsson 1998; Söderberg

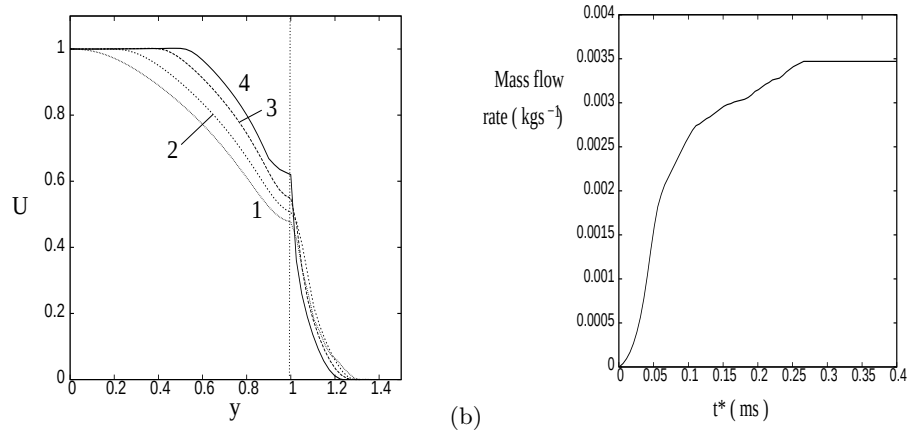

FIGURE 2. Plot of (a) the normalised velocity profiles, taken at 0.1 mm from the nozzle exit, for the CFD simulation with $q \approx 1/45$ for an axisymmetric jet with dimensional maximum velocity of 1- 44 ms^{-1}, 2- 81 ms^{-1}, 3- 182 ms^{-1} and 4- 340 ms^{-1}. The fluid interface is denoted by the vertical dotted line. Panel (b) gives the experimental mass flow rate used to generate result 4 of panel (a). Note that the mass flow rate has been modified to enter a steady state for $t^* > 2.5 \times 10^{-4}$ s. In this simulation $\rho_{\text{fuel}} = 850$ kgm^{-3}, the pressure inside the cylinder is 2 Mpa and the initial temperatures of the fuel and air are 355 K.

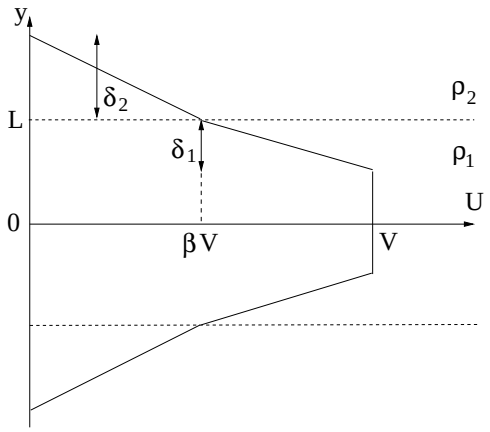

FIGURE 3. Plot of the piecewise velocity profile $U(y)$, where the thickness of the liquid jet is $2L$. The density of the liquid layer is ρ_1 and has a shear layer width of δ_1 while the air density is ρ_2 and has a shear layer thickness δ_2. The parameter $\beta \in [0, 1]$ defines the jet velocity at the fluid interface, normalized by V.

2003), but the current paper is the first to examine the stability properties of such a realistic profile using the spatio–temporal stability analysis approach.

The piecewise linear velocity profile in figure 3 is symmetric about $y = 0$, hence we need only to consider half the jet, of which the top half has the form

$$U(y) = \begin{cases} 0 & y > L + \delta_2, \\ -\frac{\beta V}{\delta_2}(y - L - \delta_2) & L + \delta_2 > y > L, \\ V - \frac{(1-\beta)V}{\delta_1}(y - L + \delta_1) & L > y > L - \delta_1, \\ V & L - \delta_1 > y > 0. \end{cases} \tag{2.1}$$

The parameter β defines the jet velocity at the fluid interface normalized by the velocity

V. It can be seen in figure 2 that β increases with increasing V by considering the velocity at the fluid interface. In figure 3 we number the layers of the profile $1-4$ from the top layer in fluid 2 to the centre layer in fluid 1. The value of L in this study will be set to $L=1$, i.e the thickness of the jet is the same as that of the nozzle, although a true value of L will be slightly smaller than unity due to a thinning of the jet as it leaves the nozzle (Domann & Hardalupas 2004). This effect is expected to be relatively small in the region of interest, so we neglect it here.

The stability of profile (2.1) to linear disturbances, in the absence of viscosity, is found by linearizing the two–dimensional Euler equations. We introduce velocity and pressure fluctuations of the form

$$(\hat{u},\hat{v},\hat{p})(x,y,t) = (U(y),0,0) + \epsilon(u(y),v(y),p(y))e^{i(\alpha x-\omega t)} + \text{ complex conjugate}, \quad (2.2)$$

into the Euler equations where $\epsilon \ll 1$ and $u,\ v,\ p = O(1)$, and time has been non-dimensionaised by L^*/U_0^*. By neglecting nonlinear terms and eliminating the pressure p and the streamwise velocity perturbation u we arrive at the Rayleigh equation (1.1) in each of the fluid layers (Drazin & Reid 1981). Here α is the wavenumber in the streamwise direction and ω is the angular frequency of the disturbance, such that $\omega/\alpha = c$ is the wave phase speed in the x direction. For high speed jets, it is likely that the fluid within the jet is close to or could even be turbulent, possibly due to the cavitation in the nozzle (Arcoumanis *et al.* 2001). However in this study we assume that any eddies in the jet are small, and so our assumption that the jet appears as a single velocity profile and can be approximated as (2.1) still holds.

The modal solutions to the Rayleigh equation can be either sinuous (even functions for v; $v(y=0)=1$, $dv/dy(0)=0$) or varicose (odd functions for v; $v(0)=0$, $dv/dy(0)=1$) modes, and as any perturbation can be made up of a linear combination of these modes we have a complete stability representation by considering these modes only. Therefore for the piecewise linear basic profile (2.1), the form of the eigenmodes can be solved for exactly in each layer. Also by using the symmetry conditions at $y=0$ and the two matching conditions

$$\Delta\left[\frac{v_j}{\alpha U_j-\omega}\right]=0, \qquad \Delta\left[\rho_j(\alpha U_j-\omega)v_j' - \rho_j\alpha U_j' v_j\right]=\chi,$$

across each velocity layer to eliminate the arbitrary constants of the problem, we can derive the dispersion relation

$$D(\alpha,\omega) = \hat{c}_4\omega^4 + \hat{c}_3\omega^3 + \hat{c}_2\omega^2 + \hat{c}_1\omega + \hat{c}_0 = 0, \quad (2.3)$$

where $\hat{c}_4$ to $\hat{c}_0$ are functions of $(\alpha,\delta_1,\delta_2,\beta,V,L,q=\rho_2/\rho_1,W)$ given in Appendix A. Here the notation is $\Delta[\ ] = [\ ]_{y_0-\epsilon}^{y_0+\epsilon}$ at the discontinuity $y=y_0$ and $\epsilon\to 0$. When the second interface condition is applied between two layers of the same fluid $\chi=0$, and $\chi = W\alpha^4\rho_1$ at the interface between the two fluids at $y=L(=1)$. The non–dimensional constant $W = We^{-1} = \sigma/(\rho_1 U_0^{*2}L^*)$, where σ is the dimensional surface tension, is the inverse of the Weber number. In the present study this parameter remains constant, but the surface tension effects appear as W/V^2 in the above dispersion relation, so as V increases the effect of surface tension reduces. Consequently we could fix $V=1$ and let W vary, but in §4 we calculate the break–up length of the jet as a function of V.

For the case of no surface tension, $W=0$, the dispersion relation reduces to

$$c_3\omega^3 + c_2\omega^2 + c_1\omega + c_0 = 0,$$

by division of the factor $(\frac{1}{2}\alpha V-\omega)$. The expressions for c_3 to c_0 can also be found in

Appendix A. For more information of the derivation of the dispersion relation, see either Drazin & Reid (1981); Schmid & Henningson (2001); Healey (2007) or Juniper (2007).

2.1. *Spatio–temporal stability analysis*

In this study we are interested in how disturbances generated at the nozzle propagate along the jet. Thus it appears that a simple temporal instability analysis for each real wavenumber α would suffice for finding unstable waves. However this analysis doesn't allow for distinguishing an absolute instability from a convective one, i.e. distinguishing a disturbance which grows at the same spatial position at which it was forced (the nozzle in this case) from one which only grows as it propagates downstream. In a steady parallel jet, an absolute instability is significant because the jet will eventually break up at the nozzle as long as enough time is allowed to pass. In this paper we examine the fluid response to the forcing in frames of reference moving at various speeds downstream (or possibly upstream) of the source of disturbances as in the problems considered by Healey (2006) and Juniper (2006).

The calculation of this response in one spatial dimension can be found in works such as Huerre (2000) and Healey (2006) and is outlined below. We assume that a time dependent forcing is turned on at $t = 0$ at the nozzle of the jet ($x = 0$), and that this can be written as the boundary condition $\hat{v}(x, 0, t) = \delta(x)\hat{f}(t)$, where $\hat{f} = 0$ for $t < 0$ (Juniper 2007). The solution for $\hat{v}(x, y, t)$ can be written as the double inverse Fourier transform

$$\hat{v}(x, y, t) = \frac{1}{4\pi^2} \int_{F_\alpha} \int_{L_\omega} \frac{f(\omega)}{D(\alpha, \omega)} v(y; \alpha, \omega) e^{i(\alpha x - \omega t)} \, d\alpha \, d\omega, \tag{2.4}$$

where $D(\alpha, \omega)$ is the dispersion relation (2.3). The integration contour F_α runs from $-\infty$ to ∞ along the real axis in the complex $\alpha-$plane, while the contour L_ω runs from $-\infty$ to ∞ above all singularities in the complex $\omega-$plane to ensure $\hat{v} = 0$ for $t < 0$.

It is possible to distinguish between convective and absolute instabilities without numerically evaluating the above double integral (Briggs 1964), by considering an impulsive forcing $\hat{f}(t) = \delta(t)$. The residue theorem can then be used to evaluate the ω integration in (2.4) as

$$\hat{v}(x, y, t) = -\frac{i}{2\pi} \sum_m \int_{F_\alpha} \frac{v(y; \alpha, \omega)}{D_\omega(\alpha, \omega_m(\alpha))} e^{i(\alpha x - \omega_m t)} \, d\alpha, \tag{2.5}$$

where ω_m is the m^{th} root of the dispersion relation. Equation (2.5) can now be evaluated by the method of steepest descent (Hinch 1991), where in the large time limit with $x/t = O(1)$ the dominant contribution to the integral comes from the particular saddle points of the function

$$g_m = \omega_m - \alpha \frac{x}{t}, \quad \text{where} \quad \frac{\partial \omega_m}{\partial \alpha} = \frac{x}{t}. \tag{2.6}$$

In this study we consider the growth of the perturbation $\hat{v}$ along all possible real characteristics $\partial\omega/\partial\alpha = x/t$, and calculate the growth rate

$$g_i = Im(g) = \omega_i - \frac{x}{t}\alpha_i,$$

where the subscript i denotes the imaginary part and we have dropped the m subscript for clarity, knowing we must consider all Riemann surfaces. The saddle points of the dispersion relation are found by simultaneously solving equations $\bar{D}(g, \alpha) = \bar{D}_\alpha(g, \alpha) = 0$, numerically using Newton iterations, where $\bar{D}(g, \alpha)$ is given by (2.3) with ω replaced by (2.6).

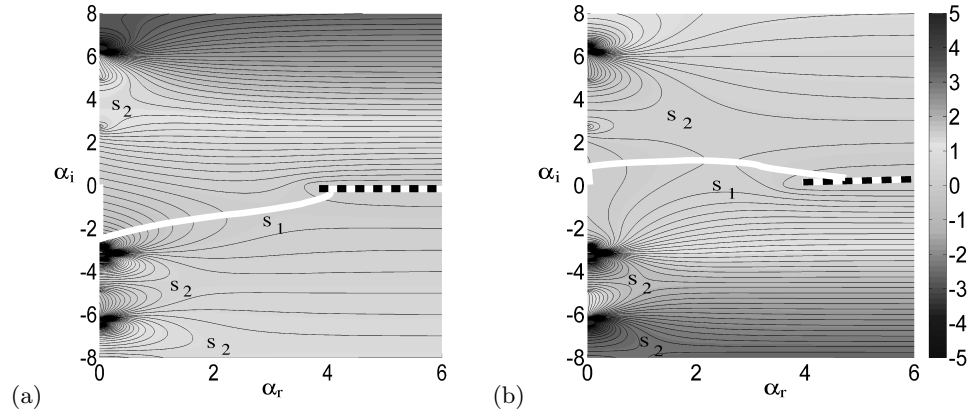

FIGURE 4. Plot of the contours of g_i in the complex $\alpha-$plane for the sinuous mode with $(\delta_1, \delta_2, q, \beta, V, W) = (0.5, 0.5, 1/500, 1/2, 1, 0)$ and (a) $x/t = 0.6$ and (b) $x/t = 0.9$. The branch cut near the real axis is marked by the dashed line while the path of integration is shown by the solid white line. The saddles are labeled s_1 and s_2 as in Juniper (2007).

2.2. *Distinction between saddle points*

In this section we show how the integral in (2.5) is evaluated, consider the two types of saddle points which contribute to the integral, and show how the saddles move around the $\alpha-$plane as we consider the growth along various x/t characteristics.

The integration path in (2.5) originally lies along the real axis in the complex $\alpha-$plane. However the method of steepest descent makes the evaluation of this contour easier by deforming the integration path to pass through particular saddle points in the $\alpha-$plane. This deformation of the integration contour can only be carried out as long as no poles or branch cuts of $g(\alpha)$ (which correspond to those of $\omega(\alpha)$) are crossed. We visualize the integration by plotting contours of g_i in the complex $\alpha-$plane and then choose an integration path which solely lies within the valleys of the saddle point (Healey 2006, 2007). A sensible choice for the inversion contour is a path which follows contours of constant $Re(g) = g_r$ (orthogonal to the contours of g_i) which is only allowed to change values of g_r at points in the $\alpha-$plane where g_i is strongly negative. This is done so as to only add a negligible contribution to the integral if we were to evaluate it numerically. If more than one saddle point with $g_i > 0$ lies on the integration path then both have to be considered for the growth rate of the disturbance. However the long time response can solely be inferred from the values of the saddle with the largest value of g_i, henceforth known as the dominant saddle point.

An example of what the contours of g_i look like in the complex $\alpha-$plane for the sinuous mode with $(\delta_1, \delta_2, q, \beta, V, W) = (0.5, 0.5, 1/500, 1/2, 1, 0)$ and $x/t = 0.6$ and $x/t = 0.9$ can be seen in figures 4(a) and (b) respectively. These parameters are chosen to give a typical velocity profile with non–zero shear layers in each fluid. The density ratio $q = 1/500$ is considered because it corresponds to cold liquid Diesel liquid fuel being injected into compressed air at about five atmospheres pressure, which is similar to the smallest density ratio in the experiments in figure 1. In this paper we adopt the notation of Juniper (2006, 2007) for the labelling of the saddle points. We denote the saddle whose position is controlled by the thickness of the shear layer and surface tension (Rees & Juniper 2009) as s_1. This saddle corresponds to waves with moderate and short wavelengths so the eigenfunctions are confined to a region close to the shear layer, so shear layer effects and surface tension are important for determining its position. The

other saddles which are controlled by the interaction of the two shear layers (Juniper 2007) are denoted as s_2 saddles. Unlike s_1 saddles, these s_2 saddles correspond to waves with long wavelengths which have wide eigenfunctions that feel the effect of both shear layers. As well as the branch cut close to the real axis (denoted by the dashed line) there are also branch cuts close to the imaginary $\alpha-$axis, which we have not shown for clarity. These branch cuts lie so close to the imaginary α–axis, such as the one which lies approximately between the origin and $\alpha_i = -3$, that they don't affect our choice of inversion contour in this study. The position of all the branch points in the $\alpha-$plane can be found by simultaneously solving equations $\bar{D}(g,\alpha) = \bar{D}_\omega(g,\alpha) = 0$, using Newton iterations. For both cases in figure 4 we note that the only saddle which lies on the contour of integration is the s_1 saddle. For $x/t = 0.6$ in figure 4(a) we see that the s_1 saddle lies below the real $\alpha-$axis, so the inversion contour comes between the two branch points at the origin, down the right hand side of the branch cut close to the imaginary axis and then passes over the s_1 saddle. The contour then passes around the branch cut close to the real $\alpha-$axis and off to infinity above the branch cut, but this is not shown here. As $x/t \to 0.5$ from above, the s_1 saddle remains the only saddle point on the integration contour and it moves to large α_r while the magnitude of g_i tends to zero. As x/t increases from 0.6 the s_1 saddle moves around the branch cut on the real α axis and onto a Riemann sheet with $\alpha_i > 0$, which can be seen for $x/t = 0.9$ in figure 4(b). In this case the dominant s_1 saddle is very close to an s_2 saddle in the upper complex plane, but an investigation of the valleys of the respective saddle points shows that for this parameter set the inversion contour cannot pass over both saddle points. Therefore as $x/t \to 1$ the s_1 saddle remains dominant and again moves to large α_r, with $g_i \to 0$, but this time above the branch cut near the real axis.

As the density ratio q is increased, the s_1 saddle moves closer to the imaginary $\alpha-$axis, but in this paper we find that the s_2 saddles do not contribute to the stability of the jet. However if the jet were confined between two solid surfaces then a further set of s_2 saddles would be introduced to the $\alpha-$plane and then as the position of the walls are varied, these s_2 saddles could become traversed by the integration contour and hence affect the stability properties of the jet as found in Juniper (2007). This, however, is not considered in the present paper.

We note that an absolute instability will occur in the jet if there exists a saddle point on the inversion contour with $g_i > 0$ for $x/t = 0$. These absolute instabilities are significant for steady jets, because eventually the flow will break down at the nozzle as long as we allow enough time to pass. Thus determining their existence for particular parameter values is very important and in the next section we calculate parameter sets with absolute instabilities that have not been documented before.

3. Stability calculations for a steady jet

In this section we present a systematic study of the convective and absolute stability properties of the velocity profile (2.1) for a wide range of parameter values, such as the shear layer thickness, surface tension and the value of the jet velocity at the fluid interface. In §4 we use the relevant results which relate to our profiles in figure 2(a) to make a connection with jet break–up lengths. Throughout this section we set $V = L = 1$ without affecting the qualitative nature of the results, and unless otherwise stated $\beta = 1/2$.

In figure 5 we plot growth rates g_i as a function of the characteristic x/t for both sinuous (results 1 and 3) and varicose (results 2 and 4) modes. For both parameter sets the varicose mode has a smaller maximum growth rate value, $g_i^{\max}$, where $g_i^{\max}$ is the maximum value of g_i, although as the shear layers thin out the growth rates for both

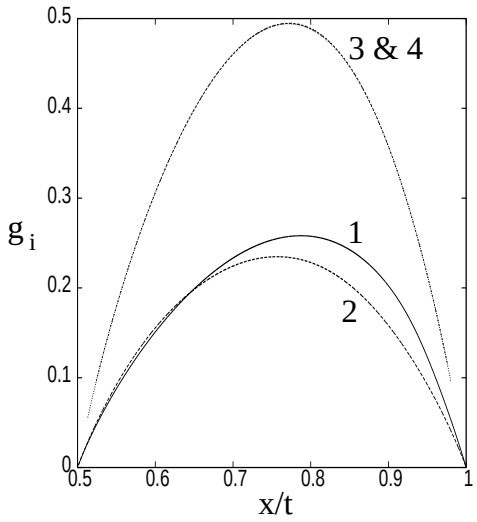

FIGURE 5. Plot of the growth rate g_i as a function of x/t for 1– the sinuous mode with $(\delta_1, \delta_2, q, W) = (0.5, 0.5, 1/500, 0)$, 2– the varicose mode with $(0.5, 0.5, 1/500, 0)$, 3– the sinuous mode with $(0.25, 0.25, 1/500, 0)$ and 4– the varicose mode with $(0.25, 0.25, 1/500, 0)$.

the sinuous and varicose modes tend to the same values, as is shown by results 3 and 4 which are indistinguishable from one another. This is because as the shear layer thins, the wavelengths shorten so the eigenfunctions decay faster with distance from the shear layer, and so whether you use $v(0) = 0$ or $v'(0) = 0$ makes very little difference. In this limit the results should approach those of an isolated mixing layer, as studied in Healey (2009), but with a modification due to the fluid interface being placed in the middle of the shear layer. In fact, the varicose modes correspond to the case of a mixing layer confined by a single plate studied in Healey (2009). As the sinuous modes have larger maximum growth rate, these modes will become unstable first and so will be significant to convective instabilities if we are interested in the initial break up of the jet. However the varicose modes also need to be considered in case they produce a shorter break–up length. The varicose modes are most significant for the absolute instabilities in the jet, and it should be noted that the varicose mode with $x/t \lesssim 0.64$ and $\delta_1 = \delta_2 = 0.5$ has a growth rate larger than the sinuous modes as well as a maximum growth rate value occurring at a lower value of x/t.

In figure 5 we also observe that as the thickness of the shear layer decreases the value of $g_i^{\max}$ increases. In fact $g_i^{\max}$ scales like δ_1^{-1} in this problem, and this can be seen as $g_i^{\max} \approx 0.25$ for $\delta_1 = \delta_2 = 0.5$ while $g_i^{\max} \approx 0.5$ for $\delta_1 = \delta_2 = 0.25$. The values of g_i for the $\delta_1 = 0.25$ result cannot be calculated for $x/t \approx 0.5$ and 1.0 because close to these values the saddle point in the $\alpha-$plane has moved to a large value of α_r, as discussed in §2.2. Thus the value of this saddle becomes difficult to calculate numerically because of numerical inaccuracies that occur in calculating the roots of the dispersion relation. This problem arises for thin shear layers and small values of q and could be overcome by evaluating the integral in (2.4) numerically and calculating the growth rate from this. However, it can be noted by studying the $\alpha-$plane that in these limits, no s_2 saddles become traversed by the integration contour, therefore it can be deduced that $g_i \to 0$ as $x/t \to 0.5$ and 1.0 as for the $\delta_1 = 0.5$ case so no difficult numerical integrals need actually be evaluated. It is found in §4 that these parts of the growth rate are not required for

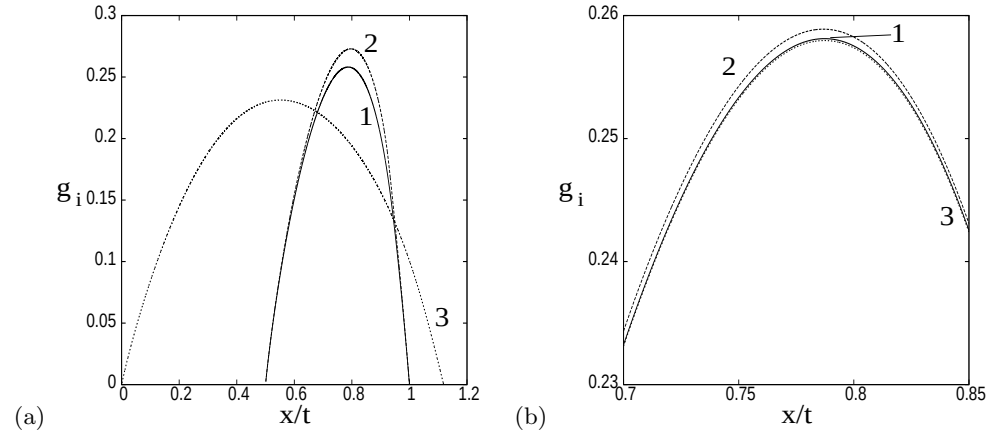

FIGURE 6. Plot of (a) the growth rate g_i for sinuous modes as a function of x/t for $(0.5, 0.5, 1/500, 0)$, $(0.5, 0.5, 1/10, 0)$ and $(0.5, 0.5, 1, 0)$ numbered $1-3$ respectively. Panel (b) shows the sinuous mode growth rates for $(0.5, 0.5, 1/500, 0)$, $(0.5, 0.1, 1/500, 0)$ and $(0.5, 0.9, 1/500, 0)$ numbered $1-3$ respectively.

calculating the break–up length for this value of q, so the calculation of these tails is irrelevant.

In figure 6(a) we plot g_i as a function of x/t for sinuous modes with the different density ratios $(0.5, 0.5, 1/500, 0)$, $(0.5, 0.5, 1/10, 0)$ and $(0.5, 0.5, 1, 0)$ numbered 1 to 3 respectively. The most striking difference between the results displayed in panel (a) is that for $q = 1$ (result 3) there is growth over a much larger range of x/t characteristics. This is significant because now there is the chance that there could be growth along the $x/t = 0$ characteristic for particular parameter values, i.e. there could now exist an absolute instability. In this case there is a very weak absolute instability for $q = 1$. As q is increased from $1/500$ to 1 the maximum value of the growth rate, $g_i^{\max}$, initially increases up to $q \approx 1/5$ before decreasing as $q \to 1$. This can be seen in figure 7(a) for $\delta_1 = \delta_2 = 0.5$. Figure 7(b) shows that the corresponding x/t value increases slightly up to $q \approx 1/4$ before also reducing as $q \to 1$. This shows that as the density difference between the two fluids becomes closer to unity, break up will occur at a later time for the same velocity profile because of the smaller growth rate, but also the disturbance will move slower along the jet. Weaker growth rates tend to delay break up, but slower axial propagation velocities tend to move break up towards the nozzle.

Figure 6(b) on the other hand shows the effect on the growth rate of varying the thickness of the outer shear layer, δ_2, when $q = 1/500$. The results show that thinning the shear layer in the less dense fluid increases the maximum growth rate by a small amount, and thickening the shear layer reduces the maximum growth rate by an even smaller amount. This small difference as δ_2 is varied demonstrates that a thickening of the outer shear layer alone cannot be responsible for the increased break–up length observed in axisymmetric Diesel jets (see the discussion in Sazhin *et al.* (2008)). As q increases the effect of the outer shear layer increases, but doesn't really become significant until $q \gtrsim 1/10$.

In figure 6(a) we find that for $q \leq 1$ the smallest value of x/t for which growth is observed is $x/t = 1/2 = \beta$. Therefore we can generate results with $g_i > 0$ for $x/t < 1/2$ by considering a fixed shear layer thickness and by varying the magnitude of the jet velocity at the fluid interface within the shear layer. This is achieved by varying the

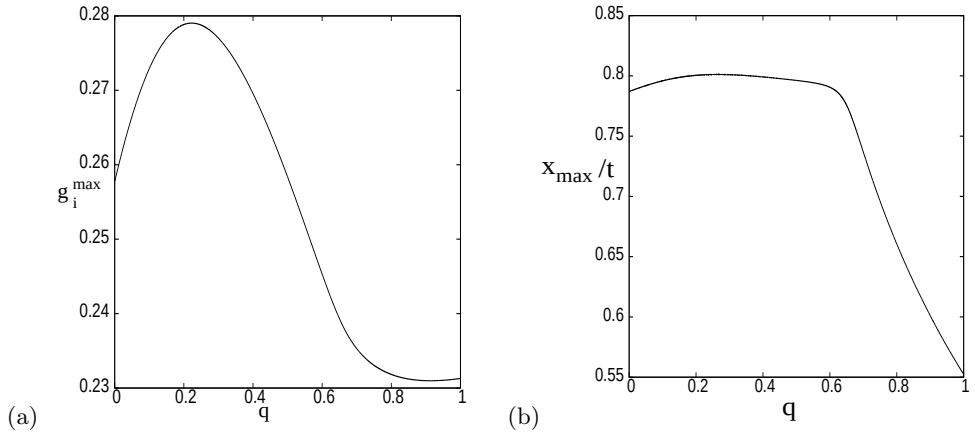

FIGURE 7. Plot of (a) the maximum growth rate $g_i^{\max}$ as a function of q for the case $\delta_1 = \delta_2 = 0.5$ and $W = 0$, while panel (b) plots the value of x/t at the maximum value.

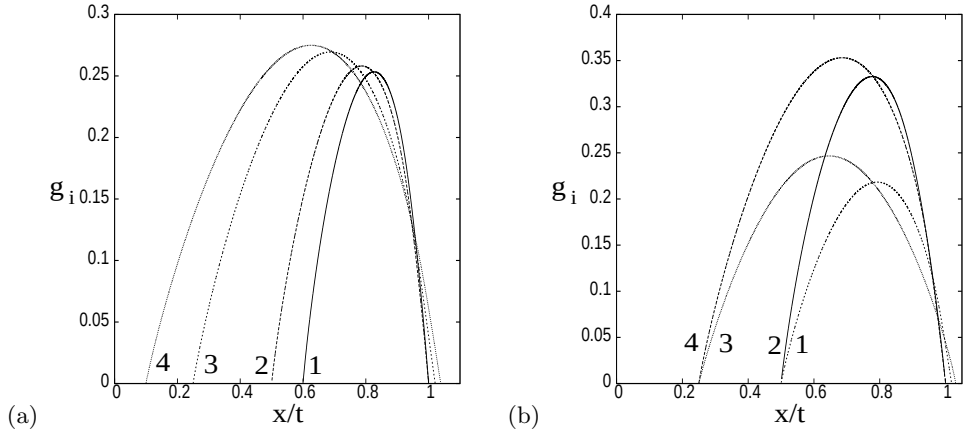

FIGURE 8. Plot of g_i as a function of x/t for sinuous modes of the velocity profile (3.1) with $q = 1/500$ and (a) $a = 1$ with $\beta = 0.6,\ 0.5,\ 0.25$ and 0.1 numbered $1 - 4$ respectively and (b) $(a, \beta) = (1.25, 0.5)$, $(0.75, 0.5)$, $(1.25, 0.25)$ and $(0.75, 0.25)$ numbered $1 - 4$ respectively.

parameter β and allowing the parameters δ_1 and δ_2 to vary as

$$\delta_1 = a(1 - \beta), \qquad \delta_2 = a\beta, \tag{3.1}$$

where a determines the thickness of the shear layer. Figure 8(a) shows that reducing β from 0.6 (result 1) to 0.5 (result 2) with $a = 1$ increases the range of x/t characteristics along which there is growth. In fact the smallest value of x/t for which there is growth is exactly β, which is verified by each of the four cases shown. We also note that the maximum value of g_i varies only slightly as β is varied, but the x/t value at the maximum moves to smaller values as β decreases. This increase in the range of x/t values with β is also seen for the varicose mode (not shown), which means that there is the possibility for an absolute instability, primarily in the varicose mode, as β is reduced. This is examined further in figure 12. We should also note that for $\beta = 0.25$ and 0.1, characteristics with $x/t > 1$ now have a positive growth rate. The implication of such solutions is discussed below. Figure 8(b) shows that different values of a give the same effect as β is varied, except that the overall growth rate is reduced as a is increased and vice versa as a is reduced.

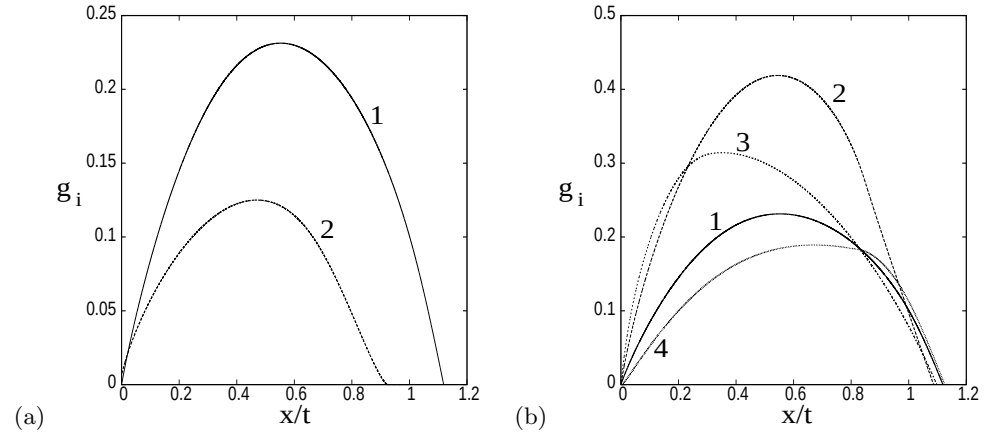

FIGURE 9. Plot of g_i as a function of x/t for (a) $(0.5, 0.5, 1, 0)$ for 1- sinuous mode and 2- varicose mode and for sinuous modes with (b) 1- $(0.5, 0.5, 1, 0)$, 2- $(0.25, 0.25, 1, 0)$, 3- $(0.5, 0.3, 1, 0)$ and 4- $(0.5, 0.7, 1, 0)$.

When we consider two fluids of equal density ($q = 1$) we find that varying parameters such as δ_2 have a greater effect on the growth rate than they did for small values of q ($= 1/500$). Figure 9(a) plots both the sinuous mode (result 1) and varicose mode (result 2) for the case $(0.5, 0.5, 1, 0)$, and these results compare to results 1 and 2 for the $q = 1/500$ case in figure 5. For the $q = 1$ results we see that there is a much larger difference between the maximum values of the growth rates of the two modes, with the sinuous mode growing more than twice as fast as the varicose mode at its maximum value. We also observe that the range of x/t characteristics where the varicose mode is larger than the sinuous mode is greatly reduced for $q = 1$ and is concentrated to a small region near $x/t = 0$. In fact for this parameter set the varicose mode gives an absolute instability (i.e. $g_i > 0$ at $x/t = 0$). The sinuous mode on the other hand has growth along characteristics which can propagate at a group velocity greater than the speed of the jet ($x/t > 1$), although the value of g_i on these characteristics is much less than the maximum value of g_i. These characteristic values would not be significant for a steady jet, as the jet is assumed to fill the whole domain $x \in [0, \infty)$. However for an accelerating jet emanating from the nozzle, the growth along these characteristics could prove important, because these wave packets would propagate along the jet, hit the front of the jet and then reflect back setting up interference with other downstream traveling wave packets which could induce break up.

So far we have focused on jets with zero surface tension, however surface tension can have a major effect on both the convective and absolute instability properties of the jet. In figure 10(a) we consider the growth rate g_i for sinuous modes as a function of x/t for the cases $(0.5, 0.5, 1/500, 0)$, $(0.5, 0.5, 1/500, 0.001)$ and $(0.5, 0.5, 1/500, 0.01)$ numbered 1–3 respectively. Here we see that increasing the effect of surface tension decreases the maximum value of the growth rate, i.e. it has a stabilizing effect on the convective instability. This is because the surface tension forces act to suppress the instability waves on the surface of the fluid thus reducing the ability of the free surface to break up. It is also interesting to note that for this small value of q, the value of x/t where the maximum value of g_i occurs increases as W is increased. In figure 10(b) we consider the effect of surface tension in the case $q = 1$, i.e. when the two fluids have equal densities, again for the case $\delta_1 = \delta_2 = 0.5$. Here we find that because q is larger than in panel (a) we require larger values of W to see a significant change to the growth rate g_i, thus we

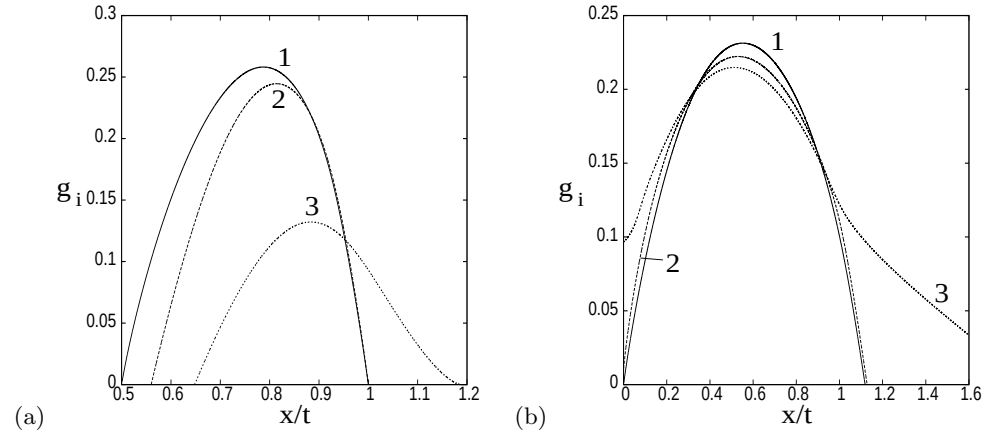

FIGURE 10. Plot of the sinuous mode growth rate g_i as a function of x/t for $(\delta_1, \delta_2, q, W) =$ (a) 1– $(0.5, 0.5, 1/500, 0)$, 2– $(0.5, 0.5, 1/500, 0.001)$ and 3– $(0.5, 0.5, 1/500, 0.01)$ and (b) 1– $(0.5, 0.5, 1, 0)$, 2– $(0.5, 0.5, 1, 0.01)$ and 3– $(0.5, 0.5, 1, 0.02)$.

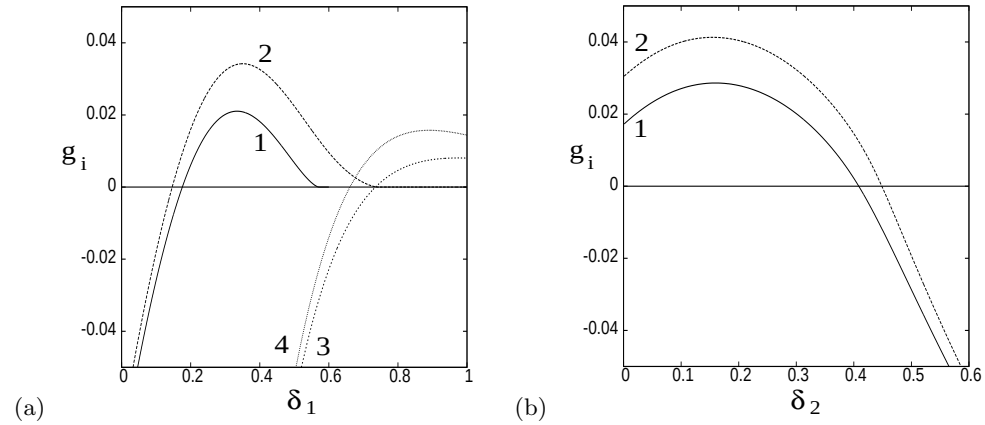

FIGURE 11. Plot of g_i for varicose modes at the s_1 saddle on the inversion contour when $x/t = 0$. In panel (a) $\delta_1 = \delta_2$ and 1– $(q, W) = (1, 0)$, 2– $(1, 0.01)$, 3– $(1/2, 0)$ and 4– $(1/2, 0.01)$. In panel (b) we fix $\delta_1 = 0.3$ and examine the value of g_i at the s_1 saddle as a function of δ_2 for 1– $(1, 0)$ and 2– $(1, 0.01)$. When this value is greater than 0 there is an absolute instability in the jet.

examine $W = 0,\ 0.01$ and 0.02 which are numbered 1–3 respectively. As for $q = 1/500$ in panel (a), the maximum value of g_i reduces as W is increased, but for $q = 1$ the x/t characteristic of the maximum growth rate moves to a smaller value. We also note that although surface tension has a stabilizing effect on the convective instability, it has a destabilizing effect on the absolute instability as result 3 in figure 10(b) shows a weak absolute instability while results 1 and 2 have no absolute instability. The destabilizing effect of surface tension for absolute instabilities has been studied by Lin & Lian (1989) and we look at its effect on our jet profiles in figures 11 and 12.

The major part of this study up to now has focused on the sinuous modes of the jet, but these modes are more stable than the varicose modes when it comes to absolute instabilities (Juniper 2006). Therefore, for the remainder of this section we focus our attention on varicose modes and investigate the conditions when they produce absolute instabilities in the jet. These are very important in the steady jets, as they tell us when there will be disturbance growth at the nozzle which eventually leads to disintegration

of the whole jet and a spray is formed. We expect an absolute instability to disintegrate the jet in this fashion because we expect similar behaviour between this flow and the wake flow of Chomaz *et al.* (1987), i.e. the jet is most unstable near the nozzle so an absolute instability at the nozzle would generate an unstable global instability in the jet. Also, any vortex rings which occur, such as in the experiments of Monkewitz & Sohn (1988), would be highly unstable to secondary instabilities at the high Reynolds numbers considered in this study, so break–up of the jet at the nozzle would be expected.

In figure 11 we plot the value of g_i at the s_1 saddle on the inversion contour for various parameter values, and where this quantity is greater than zero we have an absolute instability in the flow. For result 1, which has $\delta_1 = \delta_2$, $W = 0$ and $q = 1$, we find that we have an absolute instability for $0.175 < \delta_1 < 0.571$. This result extends the work of Juniper (2007) who suggests that a shear layer in the jet is not hugely significant to its absolute stability properties, therefore he only considered the $\delta_1 = 0$ case which gives no absolute instability for the parameter range considered here. However figure 11(a) clearly shows that increasing the thickness of the shear layer will produce absolute instability, and when the shear layer becomes too wide the absolute instability stabilizes again. Result 2 shows that increasing the surface tension ($W = 0.01$) increases the range of values of δ_1 for which there is an absolute instability to $0.146 < \delta_1 < 0.743$. It also increases the magnitude of the absolute instability as discussed in Lin & Lian (1989) and earlier in this section. Results 3 and 4 show the same absolute instability phenomena except with $q = 1/2$. In this case the absolute instability occurs for a larger δ_1 value, and even extends to $\delta_1 = 1$ where the profile becomes an triangular jet. Note that this result is the opposite of that observed by Srinivasan *et al.* (2010) who found that for low density jets ($q > 1$) the absolute instability occurs as $\delta_1 \to 0$ and becomes convectively unstable as δ_1 increases.

In figure 11(b) we fix $\delta_1 = 0.3$ with $q = 1$ and investigate how varying the outer shear layer δ_2 affects the absolute instability. From figure 11(a) we know that $\delta_2 = 0.3$ for this parameter set leads to an absolute instability, but figure 11(b) shows that reducing the thickness of the outer shear layer increases the absolute instability down to $\delta_2 = 0.160$ and then the absolute instability reduces as $\delta_2 \to 0$ still giving an absolute instability at $\delta_2 = 0$. Increasing δ_2 from 0.3 just reduces the absolute instability and at $\delta_2 = 0.408$ the absolute instability stabilizes. Result 2 shows the destabilizing effect of $W = 0.01$. For the results in figure 11 we found that reducing q much below $1/2$ removed the absolute instability, so for dense jets the flow is only convectively unstable.

In figure 12(a) we examine the absolute instability properties of the fixed shear layer profile (3.1) with $a = 8/5$ where we vary the velocity at the fluid interface, effectively varying the position of the fluid interface relative to a fixed shear layer, for the density ratio $q = 1/2$. We plot the value of g_i at the s_1 saddle, which lies on the inversion contour, as a function of β. This profile was chosen because from figure 11(a) we know that this profile, with $\beta = 1/2$, has an absolute instability with $W = 0$. We see that increasing β enhances the absolute instability up to $\beta = 0.658$, while reducing β only stabilizes the absolute instability and when $\beta = 0.440$ the absolute instability has vanished and the flow is only convectively unstable. Here, setting $W = 0.01$ (result 2) does increase the range of β for which there is an absolute instability, but only slightly, and it also shifts the position of the maximum absolute instability to a smaller value of β. Figure 12(b) shows that absolute instabilities in jets with $q < 1$ tend to only occur for values of $\beta \lesssim 0.7$ when $\delta_1 = \delta_2 = 0.8$. Therefore for the CFD profiles from figure 2(a) that we consider in §4, we may not encounter an absolute instability. However this study is still significant to other jets where β might be less than 0.7 due to the physical properties of the fluids being considered.

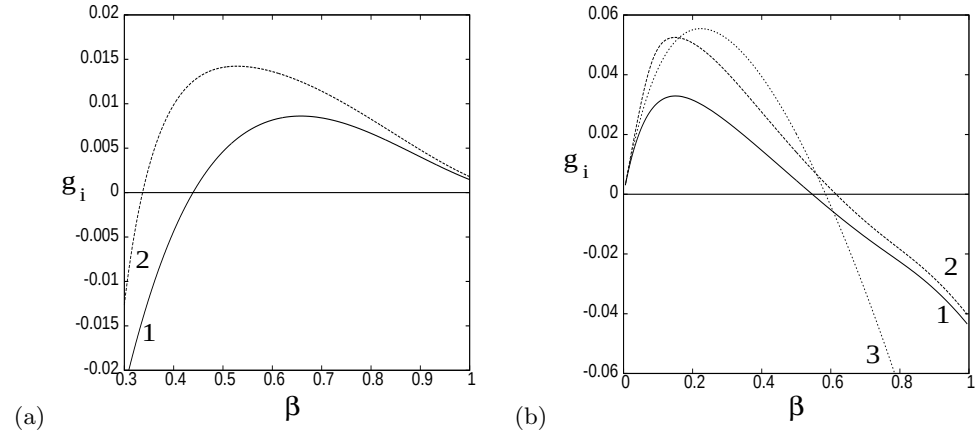

FIGURE 12. Plot of the value of g_i for the varicose mode at the s_1 saddle on the inversion contour when $x/t = 0$. For panel (a) the velocity profile is fixed by the parameters (3.1) with $a = 8/5$, $q = 1/2$ and 1– $W = 0$ and 2– $W = 0.01$, while for panel (b) $\delta_1 = \delta_2 = 0.8$ and 1– $(q, W) = (1/2, 0)$, 2– $(1/2, 0.01)$ and 3– $(1/10, 0)$. The value of g_i is plotted as a function of β, and an absolute instability develops when g_i is greater than 0.

We have now extended the study of the stability properties of a steady planar jet and identified some new phenomena associated with the inclusion of the shear layer at the jet edge. In the next section we use these results to help to explain the experimental jet break up results seen in figure 1.

4. Break–up length calculations

In this section we use the stability results from §3 to estimate break–up lengths of liquid jets. Experiments, such as those by Hiroyasu *et al.* (1982), show that a liquid jet injected from a nozzle has a break–up length which increases for small injection velocities, reaches a maximum value, and then levels off for large velocities, see figure 13 from their study or figure 1 of this study. The jets in these experiments were axisymmetric water jets injected into pressurized nitrogen, where the injection process was long enough to justify our assumption that the jets are essentially steady, and so our steady theory can be used to explain the results. The proposed model in this paper includes several undetermined parameters intended to model physical effects beyond the scope of the present study, such as the role of nonlinearity in break up. In principle, improved quantitative agreement could be sought through empirically adjusting the parameters to fit the data better, but this is not the approach we have taken nor is that the goal of this research, our intention is to obtain a qualitative understanding of the important physical processes. This limitation of our goal is partly related to the fact that Hiroyasu *et al.* (1982) considered axisymmetric jets while our model was developed for planar jets.

We examine how the parameters used in §3 affect the jet break–up length by studying four different profiles. Before discussing the profiles we first need to relate the parameters δ_1, δ_2 and β to the maximal velocity V of the jet. By considering the CFD results in figure 2 we can estimate these parameters.By considering these parameters in figure 13 we can see that δ_1 has the approximate form

$$\delta_1 = \delta_\infty + \delta' V^{-1/2}, \tag{4.1}$$

to leading order, where $\delta' + \delta_\infty$ is the non–dimensional thickness of the shear layer of the jet when $V = 1$ and δ_∞ is the thickness of the shear layer in the limit $V \to \infty$. This

Max velocity (ms^{-1})	β	δ_1	δ_2
44	0.48	0.85	0.27
81	0.49	0.77	0.26
182	0.56	0.60	0.24
340	0.63	0.44	0.23

TABLE 1. The approximate values of δ_1, δ_2 and β for the CFD simulations shown in figure 2(a).

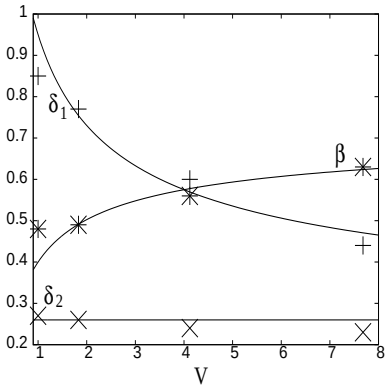

FIGURE 13. Plot of the normalized data from table 1 with the profile 1 approximations.

result also agrees with the experimental results of Marmottant & Villermaux (2004) who plot the velocity profiles of an air jet injected into static air and again find that the shear layer in the jet is proportional to $V^{-1/2}$. The variation of β with V is much smaller than for δ_1, however it still increases with increasing V, and this variation has an effect on the break–up length calculations. We fix the parameter δ_2 with respect to V, as this is approximately true for the CFD calculations. Note here that as V is varied the parameters that depend upon V are also varied, such as the surface tension effects, which appear as W/V^2 in the dispersion relation (2.3).

The four profiles we examine in this section are the following

$$\begin{aligned}
&\text{Profile 1}: \quad \delta_1 = 0.2 + 0.75V^{-1/2}, \quad \delta_2 = 0.26, \quad \beta = 0.75 - 0.35V^{-1/2},\\
&\text{Profile 2}: \quad \delta_1 = \delta_2 = 0.2 + 0.75V^{-1/2}, \quad \beta = 0.5,\\
&\text{Profile 3}: \quad \delta_1 = 0.2 + 0.75V^{-1/2}, \quad \delta_2 = 0.26, \quad \beta = 0.5,\\
&\text{Profile 4}: \quad \delta_1 = 0.8(1-\beta), \quad \delta_2 = 0.8\beta, \quad \beta = 0.75 - 0.35V^{-1/2},
\end{aligned}$$

Profile 1 gives a profile the parameters δ_1, δ_2 and β which fit the table 1 data. The values in table 1 are estimated at the dotted fluid interface in figure 2 and then profile 1 is generated by fitting curves through the data, as shown in figure 13. Note that we have non–dimensionalised the data in table 1 by the velocity of the slowest jet. A different non–dimensionalisation would have lead to different functions δ_1, δ_2 and β. Profiles 2–4 pull out particular characteristics from profile 1, so that their individual effects on the break–up length can be investigated. Profile 2 fixes the value of β, and allows both δ_1 and δ_2 to thin with V, highlighting the effect of reducing δ_1 in the small q limit where the

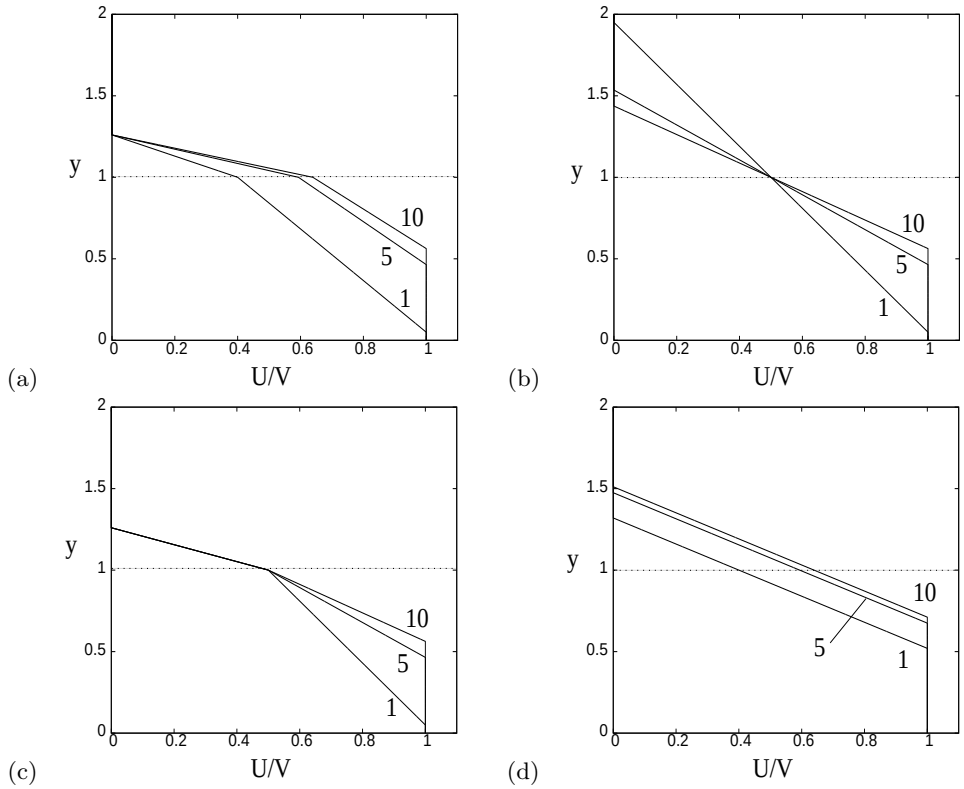

FIGURE 14. Plot of velocity profiles 1–4 in panels (a)–(d) at $V = 1,\ 5$ and 10. The dotted line indicates the fluid interface.

effect of δ_2 is small (see figure 6(b)). Profile 3 is like profile 2, but now we fix $\delta_2 = 0.26$ so that comparisons with profile 2 will show how variations in δ_2 affect the break–up length for q close to unity, where this effect is significant. Also this profile shows the effect of fixing β when compared to profile 1. Profile 4 allows us to investigate the effect of allowing β to increase on the break–up length by fixing the shear layer profile and increasing β with V. One point to note is that profiles 1–4 have been chosen to approximately coincide in the $V \to \infty$ limit, and plots of each profile at $V = 1,\ 5$ and 10 can be seen in figure 14.

The actual break–up length calculation is not a stability problem, it is a transition problem, where we wish to calculate the position at which the initial disturbance from the nozzle has reached some threshold amplitude where the disturbance can no longer be assumed to be a linear perturbation to the basic jet velocity and nonlinear effects occur. We are concerned with calculating the disturbance amplitude relative to a range of basic flow velocities, so we expect that the quantity $|\hat{v}|_{\max}/|V|$ will be relevant in estimating the position when nonlinearity starts to dominate, and we assume further that this will be a pre–cursor to rapid jet break–up. The subscript max above means maximising over the y direction. This ratio was studied by Shen (1961) who used it in unsteady flows to determine whether or not the flow was instantaneously stable or unstable. Therefore we calculate when the ratio $|\hat{v}|_{\max}/|V|$ reaches some critical value and we say that at this point break up has occurred. It is equally possible to consider the ratio of the streamwise disturbance velocity and the basic velocity $|\hat{u}|_{\max}/|V|$ or the ratio of the disturbance kinetic energy to the base flow kinetic energy, but this would just correspond

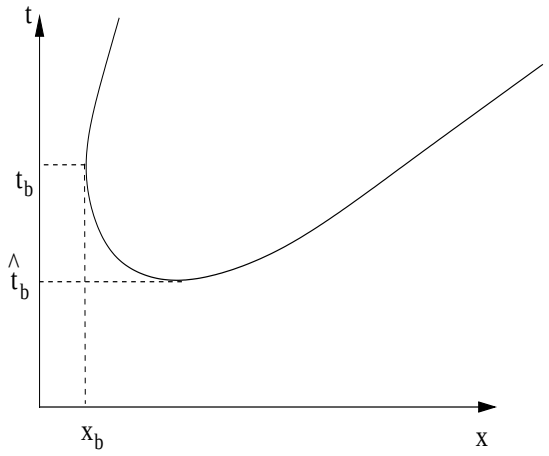

FIGURE 15. Schematic diagram of the $x-t$ plane showing the definition of the break–up length x_b, the corresponding break–up time t_b and the initial break–up time $\hat{t}_b$.

to choosing a different critical threshold value. The threshold amplitude is unknown; we have chosen $|\hat{v}_b|_{\max}/|V| = 40\tilde{v}_0$ in this paper where $|\hat{v}_b|_{\max}$ is the disturbance amplitude that triggers jet break up and $\tilde{v}_0 = |v_0|_{\max}/|V|$ is the initial disturbance amplitude ratio. Thus we assume the initial amplitude of the eigenfunction grows linearly with $|V|$. It may turn out that this is not the case, and in general $|v_0|_{\max} = f(|V|)$ for some function f, however there is no experimental evidence to determine this function, and so fixing $|v_0|_{\max}/|V|$ reduces the number of parameters we have to consider, as well as being a sensible assumption, as the initial disturbance amplitude is likely to increase with jet velocity. A 40 fold amplification of the eigenmode may not be the correct value for break–up, but changing this value will only have a quantitative effect on the results presented in this section, and the overall trend of the results will be the same. Typically the amplification factor is a function of q, but we fix it in this study as we are only seeking qualitative agreement with experiments.

Under these assumptions, the ratio of the initial disturbance amplitude, $|v_0|_{\max}$, to the amplitude of the jet at break–up along the characteristic $x/t = C =$ constant is found from the method of steepest descent to be the solution of

$$\frac{|\hat{v}_b|_{\max}}{|V|} = \frac{|v_0|_{\max}}{|V|[t_b(C)|\partial^2 g/\partial\alpha^2|_{x/t=C}]^{1/2}} \exp\left(g_i(C)t_b(C)\right), \tag{4.2}$$

where $t_b(C)$ is the time of break–up along the particular characteristic C and $v_0(y)$ is the corresponding initial disturbance eigenfunction at the saddle point corresponding to $x/t = C$, whose magnitude can be adjusted. Then for a steady jet the break–up length along the characteristic $x/t = C$ is given by the following formula:

$$x_b^{s,v}(C) = \left.\frac{\partial\omega}{\partial\alpha}\right|_{x/t=C} t_b^{s,v}(C) = Ct_b^{s,v}(C), \tag{4.3}$$

where $\partial\omega/\partial\alpha$ evaluated at the dominant saddle point on $x/t = C$ is equal to C. The superscript s or v signifies whether this is the break–up length is for the sinuous or varicose mode. The actual break–up length x_b is then taken to be the $\min(x_b^s, x_b^v)$ over every characteristic $x/t = C$ with $g_i(C) > 0$. A schematic diagram of the $x-t$ plane defining x_b and t_b is given in figure 15.

In figure 16(a) we see that $x_b(V)$ for $q = 1/500$ (result 1) shows an increase in value

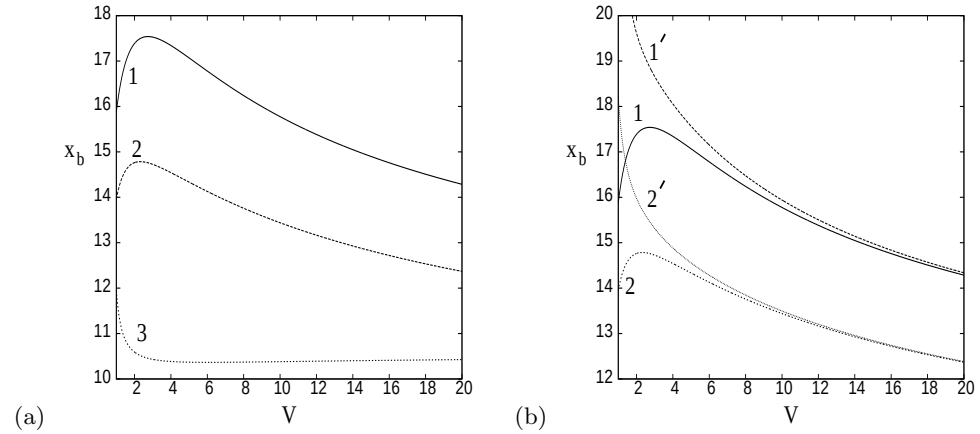

FIGURE 16. Plot of (a) 1– $x_b(V)$ for $(q, W) = (1/500, 0)$, 2– $x_b(V)$ for $(1/10, 0)$ and 3– $x_b(V)$ for $(1/2, 0)$ all for profile 1. Panel (b) replots results 1 and 2 of panel (a), and the primes denote the corresponding results with $W = 0.01$.

for small V before decreasing as V continues to increase. In these results the break–up length is dominated by the sinuous modes of the jet. As q is increased to $q = 1/10$ (result 2) we see a similar structure as for $q = 1/500$, except now the overall break–up length is reduced. When these results are compared to the experimental results in figure 1 (or figure 13 of Hiroyasu *et al.* (1982)), we see qualitative agreement. The results in Hiroyasu *et al.* (1982) were plotted for various gas pressures P_a into which the fluid is injected. Increasing P_a corresponds to increasing q, and the results in figure 13 of Hiroyasu *et al.* (1982) correspond to $q = 1/1000,\ 1/100,\ 1/30$ and $1/25$ from top to bottom respectively. In figure 16(a), the $q = 1/2$ result shows a slightly different behaviour, with $x_b(V)$ reducing and leveling off as V increases. The main reason for this is because the parameters δ_1, δ_2 and β are actually functions of q as well as V, so a jet with $q = 1/2$ may have a different profile than that given by profile 1. However we have ignored this extra complication in this study for simplicity.

Figure 16(b) replots the $q = 1/500$ and $q = 1/10$ results of figure 16(a) and includes the corresponding results with $W = 0.01$ denoted by primes. For both results the inclusion of surface tension stabilizes the flow and causes the break–up length to increase, also the increase in x_b for small V is removed. Note that as V is increased the effect of surface tension decreases and the $W \neq 0$ results tend to the $W = 0$ results rapidly, due to surface tension occurring as W/V^2 in the dispersion relation (2.3). The surface tension from the experiments of Hiroyasu *et al.* (1982) is $O(10^{-4})$, so the surface tensions we consider here are larger than the experiments.

In figure 17 we plot $x_b(V)$ for profiles 2–4 with (a) $(q, W) = (1/500, 0)$ and (b) $(1/2, 0)$. In panel (a) the results for profile 3 are not plotted as they cannot be distinguished from the profile 2 results for this value of q. This confirms the unimportance of the value of δ_2 at this particular density ratio. For curve 1 in figure 17(a), we already know that thinning the shear layer δ_1 causes the maximum growth rate to increase (see figure 5) which itself causes the break–up length to reduce as a function of V. For this value of q, the value of x/t along which break–up occurs is within 5% of the characteristic along which g_i is maximum, see figure 18(a). However, increasing the fluid velocity at the fluid interface (profile 4, curve 2) in figure 17(a) causes the break–up length to increase slightly at small values of V before remaining approximately constant over the rest of the range. This is due to the maximum growth rate reducing as β increases (see figure 8). In figure 17(b)

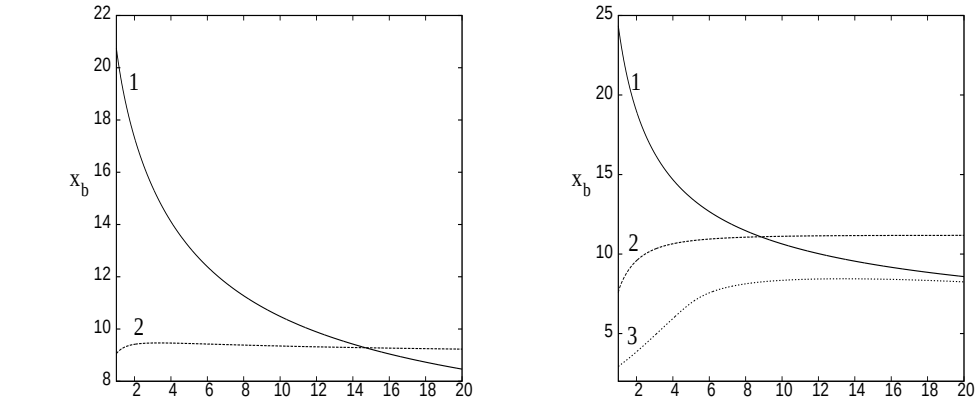

FIGURE 17. Plot of (a) 1– $x_b(V)$ for profile 2 and 2– $x_b(V)$ for profile 4 for $(q, W) = (1/500, 0)$. Panel (b) shows 1– $x_b(V)$ for profile 2, 2– $x_b(V)$ for profile 4 and 3– $x_b(V)$ for profile 3 for $(1/2, 0)$.

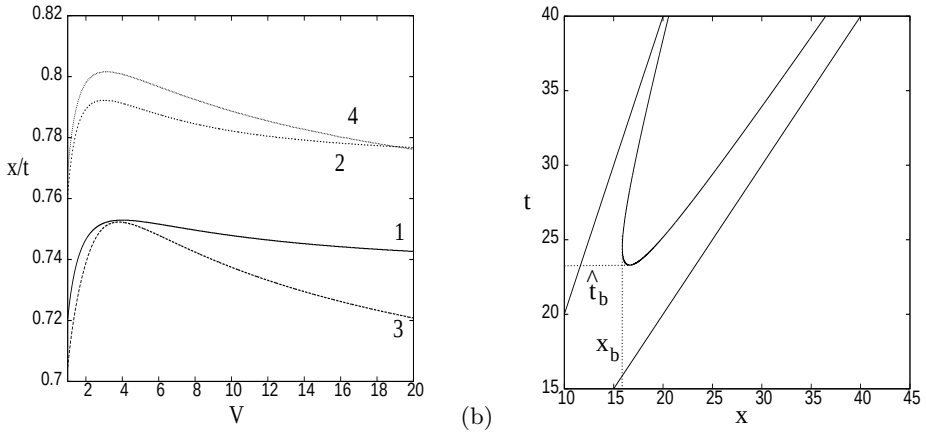

FIGURE 18. Plot of (a) the value of x/t along which break up occurs for the sinuous mode of profile 2 for 1– $(1/500, 0)$ and 3– $(1/2, 0)$. Results 2 and 4 give the corresponding characteristics for the maximum value of the growth rate. Panel (b) plots the $x - t$ plane for the sinuous mode of result 1 figure 16(a) at $V = 1$. The curve gives the contour along which $|\hat{v}|/|V| = |\hat{v}_b|/|V|$, while the solid straight lines give the edges of the wavepacket. The dotted lines give the values of x_b and the initial time of break up $\hat{t}_b$..

for $q = 1/2$ we see similar results for profile 2 (curve 1) and profile 4 (curve 2), but now break up occurs along characteristics further away from the characteristic along which g_i is maximum with approximately 8% difference in characteristic values (see figure 18(a)). Therefore we cannot just examine how the maximum growth rate varies with V to give an indication of how x_b will vary. These differences can also be seen in the $x - t$ plot of figure 18(b) for the $q = 1/500$ result from figure 16(a). Here we plot the contour at the edges of the wavepacket and the contour where $|\hat{v}|/|V| = |\hat{v}_b|/|V|$ to show where break–up occurs. We can see the clear difference between the break–up lengths given by x_b and the position where break up first occurs. In figure 17(b) we plot x_b for profile 3, and see that unlike for $q = 1/500$ the results are qualitatively different than those of profile 2. Here there is an increase in x_b initially before leveling off for larger velocities, therefore at this density ratio the shear layer in the lighter fluid is significant.

In this section we have shown qualitative agreement between our theoretical predictions

and the experimental results of Hiroyasu *et al.* (1982), including a possible explanation of the turning point behaviour in $x_b(V)$ that can arise at some parameter combinations. We have demonstrated that the turning point can occur even when $W = 0$, so this behaviour is not a surface tension effect. However the current results need to be extended to axisymmetric jets to fully confirm this.

5. Conclusions and discussion

In this paper we have used a spatio–temporal stability analysis to examine the linear stability of a steady two–dimensional planar liquid jet which has a shear layer in both the inner and outer fluid. Using a piecewise linear velocity profile we showed that for two fluids with a density ratio $q = 1/500$ (which corresponds approximately to cold Diesel fuel injecting into compressed air at 5 atmospheres) the important characteristic of the velocity profile was the size of the shear layer in the denser fluid, as this had the largest effect on the growth rate of disturbances. The width of the shear layer in the less dense fluid on the other hand made no significant contribution at this value of q. However as the density ratio of the two fluids was increased the width of the second shear layer contributed more significantly to the stability properties of the jet, and consequently the break–up length properties. Surface tension was found to stabilize the convective stability properties of the jet by reducing the maximum growth rate value for a given velocity profile.

We investigated the effect of thickening the liquid shear layer on the absolute instability of the jet, and found that the finite shear layer produces an absolute instability in jets with smaller values of the density parameter than was found in the work of Juniper (2006) who considered only infinitely thin shear layers. Juniper (2006) found that absolute instability occurs for $q \gtrsim 1.25$, while we have shown that an absolute instability occurs for at least $q > 0.5$. Therefore, the structure of the shear layer is important in these type of problems. The work in the present paper also found that increasing the fluid velocity at the fluid interface within the shear layer of the jet can destabilize the absolute instability but ultimately the flow is convectively unstable for the values of β observed in our CFD calculations (where β is the ratio of the fluid velocity at the interface to the maximum velocity). In the case of absolute instabilities, surface tension was found to act as a destabilizing effect in agreement with the work of Lin & Lian (1989).

Using the spatio–temporal analysis we have been able to demonstrate that the break–up length of a jet reduces as the shear layer in the jet thins, while the break–up length increases as the magnitude of the fluid velocity at the fluid interface increases. By combining these two effects into a profile which describes more accurately what occurs in a real jet, we have been able to produce qualitative agreement with the experiments of Hiroyasu *et al.* (1982).

We note that in the axisymmetric jet case, surface tension has a destabilizing role at small jet velocities because it can trigger the pinch off of drops of radius comparable to the radius of the jet, so this may also act to reduce break–up lengths at small jet velocities, but this may not be an important mechanism at parameters relevant to fuel injection. When extending this work to axisymmetric jets we also have to be aware that the wave with zero azimuthal wavenumber behaves like the varicose mode of the planar jet case and is destabilized by surface tension, so some differences in the the results may be observed (Juniper 2008). This however is beyond the scope of the present paper.

The authors would like to thank Cyril Crua for supplying the experimental data for the CFD simulations. This work is supported by the EPSRC under grants EP/F069855/1,

EP/G000034/1 and EP/F069855/1. We would also like to thank the anonymous referees whose comments led to an improved version of this paper.

Appendix A. The dispersion relation

The dispersion relation in §2 has the form

$$\hat{c}_4\omega^4 + \hat{c}_3\omega^3 + \hat{c}_2\omega^2 + \hat{c}_1\omega + \hat{c}_0 = 0$$

where

$$\begin{aligned}
\hat{c}_4 &= -c_3,\\
\hat{c}_3 &= \beta\alpha V c_3 - c_2,\\
\hat{c}_2 &= \beta\alpha V c_2 - c_1 - T_3(T_1^2-1)(1+T_2)(T_3-1)W\alpha^4,\\
\hat{c}_1 &= \beta\alpha V c_1 - c_0 - \left[\frac{\beta V}{\delta_2}T_3(T_2-T_3)(T_1^2-1)\right.\\
&\quad \left. + (1+T_2)(T_3-1)\left(\frac{(1-\beta)VT_1^2}{\delta_1} - T_3\left(\alpha V(T_1^2-1) + \frac{(1-\beta)VT_1}{\delta_1}\right)\right)\right]W\alpha^4,\\
\hat{c}_0 &= \beta\alpha V c_0 - \frac{\beta V}{\delta_2}(T_2-T_3)\left[\frac{(1-\beta)VT_1^2}{\delta_1} - T_3\left(\alpha V(T_1^2-1) + \frac{(1-\beta)VT_1}{\delta_1}\right)\right]W\alpha^4,
\end{aligned}$$

with

$$\begin{aligned}
c_3 &= -(T_1^2-1)(1+T_2)(T_3-1)(qT_3+1),\\
c_2 &= (1+T_2)(qT_3+1)(T_3-1)\left((1+\beta)\alpha V(T_1^2-1) + \frac{(1-\beta)VT_1}{\delta_1}\right)\\
&\quad + \frac{\beta V}{\delta_2}(T_1^2-1)\left(T_3(1-q) - T_2(1-qT_3^2)\right) + \frac{(1-\beta)VT_1^2}{\delta_1}(1+T_2)(T_3+q)(1-T_3)\\
&\quad + V\left(\frac{(1-\beta)}{\delta_1} - \frac{\beta q}{\delta_2}\right)(T_1^2-1)(1+T_2)T_3(T_3-1),\\
c_1 &= \beta\alpha V\left[(1+T_2)(qT_3+1)(1-T_3)\left(\alpha V(T_1^2-1) + \frac{(1-\beta)VT_1}{\delta_1}\right)\right.\\
&\quad \left. + \frac{\beta V}{\delta_2}(T_1^2-1)(T_2(1-qT_3^2) - T_3(1-q)) + \frac{(1-\beta)VT_1^2}{\delta_1}(1+T_2)(T_3-1)(T_3+q)\right]\\
&\quad + \frac{\beta V}{\delta_2}\left(\alpha V(T_1^2-1) + \frac{(1-\beta)VT_1}{\delta_1}\right)(T_2(1-qT_3^2) - T_3(1-q))\\
&\quad + \frac{\beta(1-\beta)V^2T_1^2}{\delta_1\delta_2}(T_3^2 - q - T_2T_3(1-q))\\
&\quad + V\left(\frac{(1-\beta)}{\delta_1} - \frac{\beta q}{\delta_2}\right)\left[(1+T_2)T_3(1-T_3)\left(\alpha V(T_1^2-1) + \frac{(1-\beta)VT_1}{\delta_1}\right)\right.\\
&\quad \left. + \frac{\beta VT_3}{\delta_2}(T_1^2-1)(T_2-T_3) + \frac{(1-\beta)VT_1^2}{\delta_1}(1+T_2)(T_3-1)\right],\\
c_0 &= \beta\alpha V\left[\frac{\beta V}{\delta_2}\left(\alpha V(T_1^2-1) + \frac{(1-\beta)VT_1}{\delta_1}\right)(T_3(1-q) - T_2(1-qT_3^2))\right.\\
&\quad \left. + \frac{\beta(1-\beta)V^2T_1^2}{\delta_1\delta_2}(T_2T_3(1-q) - T_3^2 + q)\right]\\
&\quad + \frac{\beta V^2}{\delta_2}\left(\frac{(1-\beta)}{\delta_1} - \frac{\beta q}{\delta_2}\right)(T_3-T_2)\left(T_3\left(\alpha V(T_1^2-1) + \frac{(1-\beta)VT_1}{\delta_1}\right) - \frac{(1-\beta)VT_1^2}{\delta_1}\right),
\end{aligned}$$

for varicose modes and

$$\begin{aligned}
\hat{c}_4 &= -c_3,\\
\hat{c}_3 &= \beta\alpha V c_3 - c_2,\\
\hat{c}_2 &= \beta\alpha V c_2 - c_1 - (T_1^2-1)(1+T_2)(T_3-1)W\alpha^4,\\
\hat{c}_1 &= \beta\alpha V c_1 - c_0 + \left[\frac{\beta V}{\delta_2}(T_2-T_3)(T_1^2-1)\right.\\
&\quad \left. - (1+T_2)(T_3-1)\left(\alpha V(T_1^2-1) - \frac{(1-\beta)V}{\delta_1}(T_1-T_3)\right)\right] W\alpha^4,\\
\hat{c}_0 &= \beta\alpha V c_0 + \frac{\beta V}{\delta_2}(T_3-T_2)\left[\alpha V(T_1^2-1) - \frac{(1-\beta)V}{\delta_1}(T_1-T_3)\right] W\alpha^4,
\end{aligned}$$

with

$$\begin{aligned}
c_3 &= (T_1^2-1)(1+T_2)(T_3-1)(T_3+q),\\
c_2 &= (1+T_2)(T_3+q)(1-T_3)\left((1+\beta)\alpha V(T_1^2-1) - \frac{(1-\beta)VT_1}{\delta_1}\right)\\
&\quad + \frac{\beta V}{\delta_2}(T_1^2-1)\left(T_2T_3(1-q) - T_3^2 + q\right) + \frac{(1-\beta)V}{\delta_1}(1+T_2)(qT_3+1)(1-T_3)\\
&\quad + V\left(\frac{(1-\beta)}{\delta_1} - \frac{\beta q}{\delta_2}\right)(T_1^2-1)(1+T_2)(1-T_3),\\
c_1 &= \beta\alpha V\left[(1+T_2)(T_3+q)(T_3-1)\left(\alpha V(T_1^2-1) - \frac{(1-\beta)VT_1}{\delta_1}\right)\right.\\
&\quad \left. + \frac{\beta V}{\delta_2}(T_1^2-1)(T_3^2-q-T_2T_3(1-q)) + \frac{(1-\beta)V}{\delta_1}(1+T_2)(T_3-1)(qT_3+1)\right]\\
&\quad + \frac{\beta V}{\delta_2}\left(\alpha V(T_1^2-1) - \frac{(1-\beta)VT_1}{\delta_1}\right)(T_3^2-q-T_2T_3(1-q))\\
&\quad + \frac{\beta(1-\beta)V^2}{\delta_1\delta_2}(T_3(1-q) + T_2(qT_3^2-1))\\
&\quad + V\left(\frac{(1-\beta)}{\delta_1} - \frac{\beta q}{\delta_2}\right)\left[(1+T_2)(T_3-1)\left(\alpha V(T_1^2-1) - \frac{(1-\beta)VT_1}{\delta_1}\right)\right.\\
&\quad \left. + \frac{\beta V}{\delta_2}(T_1^2-1)(T_3-T_2) + \frac{(1-\beta)VT_3}{\delta_1}(1+T_2)(T_3-1)\right],\\
c_0 &= \beta\alpha V\left[\frac{\beta V}{\delta_2}\left(\alpha V(T_1^2-1) - \frac{(1-\beta)VT_1}{\delta_1}\right)(T_2T_3(1-q) - T_3^2 + q)\right.\\
&\quad \left. + \frac{\beta(1-\beta)V^2}{\delta_1\delta_2}(T_2(1-qT_3^2) - T_3(1-q))\right]\\
&\quad + \frac{\beta V^2}{\delta_2}\left(\frac{(1-\beta)}{\delta_1} - \frac{\beta q}{\delta_2}\right)(T_2-T_3)\left(\alpha V(T_1^2-1) - \frac{(1-\beta)V}{\delta_1}(T_1-T_3)\right),
\end{aligned}$$

for sinuous modes, where $T_1 = \tanh(\alpha(L-\delta_1))$, $T_2 = \tanh(\alpha(L+\delta_2))$, $T_3 = \tanh(\alpha L)$ and $q = \rho_2/\rho_1$.

REFERENCES

Arcoumanis, C., Gavaises, M., Flora, H. & Roth, H. 2001 Visualisation of cavitation in diesel engine injectors. *Mec. Ind.* **2**, 375–381.

Batchelor, G. K. & Gill, A. E. 1962 Analysis of the stability of axisymmetric jets. *J. Fluid Mech.* **14**, 529–551.

Briggs, R. J. 1964 *Electron–Stream Interaction with Plasmas*. MIT Press.

Chomaz, J. M., Huerre, P. & Redekopp, L. G. 1987 Models of hydrodynamic resonances in separated shear flows. In:*Proc. 6th Symp. on Turbulent Shear Flows. Toulouse, France* pp. 321–326.

Crua, C. 2002 Combustion processes in a diesel engine. *PhD Thesis, University of Brighton, Brighton, United Kingdom* .

Domann, R. & Hardalupas, Y. 2004 Breakup model for accelerating liquid jets. *Proceedings of 42nd AIAA Areospace Science Meeting and Exhibition,* Reno, Nevada, Paper AIAA–2004–1155 .

Drazin, P. G. & Reid, W. H. 1981 *Hydrodynamic Stability*. Cambridge University Press.

Eggers, J. & Villermaux, E. 2008 Physics of liquid jets. *Rep. Prog. Phys.* **71**, 036601–1–79.

Esch, R. E. 1957 The instability of a shear layer between two parallel streams. *J. Fluid Mech* **3**, 289–303.

Ferziger, J. H. & Peric, F. M. 2004 *Computational Methods for Fluid Dynamics, Third ed.*. Springer (Berlin).

Funada, T., Joseph, D. D. & Yamashita, S. 2004 Stability of a liquid jet into incompressible gases and liquids. *Int. J. Multiphase Flow* **30**, 1279–1310.

Hagerty, W. W. & Shea, J. F. 1955 A study of the stability of plane fluid sheets. *J. Appl. Mech.* **22**, 509–514.

Hashimoto, H. & Suzuki, T. 1991 Experimental and theoretical study of fine interfacial waves on thin liquid sheet. *JSME Int. J. Series II* **34** (3), 277–283.

Healey, J. J. 2006 A new convective instability of the rotating-disk boundary layer with growth normal to the disk. *J. Fluid Mech.* **560**, 279–310.

Healey, J. J. 2007 Enhancing the absolute instability of a boundary layer by adding a far-away plate. *J. Fluid Mech.* **579**, 29–61.

Healey, J. J. 2009 Destabilizing effects of confinement on homogeneous mixing layers. *J. Fluid Mech.* **623**, 241–271.

Heurre, P. & Monkewitz, P. A. 1990 Local and global instabilities in spatially developing flows. *A. Rev. Fluid Mech.* **22**, 473–537.

Heywood, J. B. 1998 *Internal combustion engine fundamentals*. McGraw–Hill (Singapore).

Hinch, E. J. 1991 *Perturbation Methods*. Cambridge University Press.

Hiroyasu, H., Shimizu, M. & Arai, M. 1982 The break–up of high speed jet in a high pressure gaseous atmosphere. *Proc. 2nd Int. Conf. on Liquid Atomization and Spray Systems* pp. 69–74.

Huerre, P. 2000 *Open shear flow instabilities. In Perspectives in Fluid Dynamics: A Collective Introduction to Current Research (ed. G. K. Batchelor, H. K. Moffat and M. G. Worster)*.. Cambridge University Press.

Juniper, M. P. 2006 The effect of confinement on the stability of two-dimensional shear flows. *J. Fluid Mech.* **565**, 171–195.

Juniper, M. P. 2007 The full impulse response of two-dimensional jet/wake flows and implications for confinement. *J. Fluid Mech.* **590**, 163–185.

Juniper, M. P. 2008 The effect of confinement on the stability of non-swirling round jet/wake flows. *J. Fluid Mech.* **605**, 227–252.

Karimi, K. 2007 Characterisation of multiple–injection diesel sprays at elevated pressures and temperatures. *PhD Thesis, University of Brighton, Brighton, United Kingdom* .

Lesshafft, L. & Huerre, P. 2007 Linear impulse response in hot round jets. *Phys. Fluids* **19**, 024102.

Li, X. & Tankin, R. R. 1991 On the temporal stability of a two–dimensional viscous liquid sheet. *J. Fluid Mech* **226**, 425–443.

Lin, S. P. & Lian, Z. W. 1989 Absolute instability of a liquid jet in a gas. *Phys. Fluids* **1** (3), 490–493.

Lin, S. P., Lian, Z. W. & Creighton, B. J. 1990 Absolute and convective instability of a liquid sheet. *J. Fluid Mech* **220**, 673–689.

Lord Rayleigh 1894 *The theory of sound, 2nd edn*. Macmillian (London).

Marmottant, P. & Villermaux, E. 2004 On spray formation. *J. Fluid Mech.* **498**, 73–111.

Monkewitz, P. A. & Sohn, K. D. 1988 Absolute instability in hot jets. *AIAA Journal* **26**, 911–916.

Raynal, L., Harion, J.-L., Favre-Marinet, M. & Binder, G. 1996 The oscillatory instability of plane variable–density jets. *Phys. Fluids* **8**, 993–1006.

Rees, S. J. & Juniper, M. P. 2009 The effect of surface tension on the stability of unconfined and confined planar jets and wakes. *J. Fluid Mech.* **633**, 71–97.

Rees, S. J. & Juniper, M. P. 2010 The effect of confinement on the stability of viscous planar jets and wakes. *J. Fluid Mech.* (in press) .

Sazhin, S. S., Crua, C., Kennaird, D. A. & Heikal, M. R. 2003 The initial stage of fuel spray penetration. *Fuel* **82** (8), 875–885.

Sazhin, S. S., Martynov, S. B., Kristyadi, T., Crua, C. & Heikal, M. R. 2008 Diesel fuel spray penetration, heating, evaporation and ignition: modelling vs. experimentation. *Int. J. Engineering Systems Morelling and Simulation* **1** (1), 1–19.

Schmid, P. J. & Henningson, D. S. 2001 *Stability and transition in shear flows*. Springer (New York).

Shen, S. F. 1961 Some considerations on the laminar stability of time-dependent basic flows. *J. Aerospace Sci.* **28**, 397–404, 417.

Söderberg, L. D. 2003 Absolute and convective instability of a relaxational plane liquid jet. *J. Fluid Mech.* **493**, 89–119.

Söderberg, L. D. & Alfredsson, P. H. 1998 Experimental and theoretical stability investigations of plane liquid jets. *Eur. J. Mech B/Fluids* **17**, 689–737.

Sreenivasan, K. R., Raghu, S. & Kyle, D. 1989 Absolute instability in variable density round jets. *Exp. Fluids* **7**, 309–317.

Srinivasan, V., Hallberg, M. P. & Strykowski, P. J. 2010 Viscous linear stability of axisymmetric low–density jets: Parameters influencing absolute instability. *Phys. Fluids* **22**, 024103.

Stone, R. 1992 *Introduction to internal combustion engines*. MacMillan (New York).

Youngs, D. L. 1982 *Time–dependent multi–material flow with large fluid distortion. In Numerical methods for fluid dynamics (ed. K. W. Morton and M. J. Baines)*. Academic Press.

Yu, M. H. & Monkewitz, P. A. 1990 The effect of non–uniform density on the absolute instability of planar inertial jets and wakes. *Phys. Fluids A* **2** (7), 1175–1181.